Materials Today Bio 26 (2024) 101035

Contents lists available at ScienceDirect

Materials Today Bio

journal homepage: www.journals.elsevier.com/materials-today-bio

Potent cancer therapy by liposome microstructure tailoring with active-to-passive targeting and shell-to-core thermosensitive features

Mengxin Zhao [a,1], Xiaodong Zhu [a,1], Bailing Li [b,1], Chenyang Yan [a,1], Cong Wu [a], Lei He [a,d], Jingyi Cao [b], Fanglin Lu [b], Han Chen [c,**], Wei Li [a,*]

[a] Department of Nanomedicine & Shanghai Key Lab of Cell Engineering, Naval Medical University, Shanghai, 200433, China
[b] Department of Cardiovascular Surgery, Changhai Hospital, Naval Medical University, Shanghai, 200433, China
[c] Department of General Surgery, 905th Hospital of People's Liberation Army Navy, Naval Medical University, Shanghai, 200433, China
[d] School of Health Science and Engineering, University of Shanghai for Science and Technology, Shanghai, 200093, China

ARTICLE INFO

Keywords:
Liposome
Microstructural tailoring
Targeting
Drug delivery
Tumor cells

ABSTRACT

Liposomes have been widely studied as drug carriers for clinical application, and the key issue is how to achieve effective delivery through targeting strategies. Even though certain cell-level targeting or EPR effect designs have been developed, reaching sufficient drug concentration in intracellular regions remains a challenge due to the singularity of functionality. Herein, benefiting from the unique features of tumor from tissue to cell, a dual-thermosensitive and dual-targeting liposome (DTSL) was creatively fabricated through fine microstructure tailoring, which holds intelligent both tissue-regulated active-to-passive binding and membrane-derived homologous-fusion (HF) properties. At the micro level, DTSL can actively capture tumor cells and accompany the enhanced HF effect stimulated by self-constriction, which achieves a synergistic promotion effect targeting tissues to cells. As a result, this first active-then passive targeting process makes drug delivery more accurate and effective, and after dynamic targeting into cells, the nucleus of DTSL undergoes further thermally responsive contraction, fully releasing internal drugs. *In vivo* experiments showed that liposomes with dual targeting and dual thermosensitive features almost completely inhibited tumor growth. Summarized, these results provide a reference for a rational design and microstructural tailoring of the liposomal co-delivery system of drugs, suggesting that active-to-passive dual-targeting DTSL can function as a new strategy for cancer treatment.

1. Introduction

The mRNA vaccine technology prepared by the liposome system can transmit accurate genetic information to antigen-presenting cells, showing the preventive effect on multiple viral targets in preclinical models, especially the potential to protect against COVID-19 [1–5]. Liposomes are phospholipid vesicles with inner aqueous space and lipid bilayers, which can entrap both lipophilic (in the bilayer membrane) and hydrophilic (in the aqueous center) compounds, allowing encapsulation of a diverse range of drugs. Moreover, chemotherapeutics based on liposomes is a feasible clinical application technology offering a long internal circulation and lower drug toxicity compared to free drugs [6]. Long-circulating liposomes have been widely deemed passive to accumulate at tumor sites by the enhanced permeability and retention effect (EPR) [7–9]. However, there still are some drawbacks to the systemic application of these traditional long-circulating liposomes, including poor pharmacokinetic profiles, incomplete local targeting, lack of deep tissue penetration, nonspecific biodistribution, and limited retention at sites of delivery [10–12]. Currently, various liposomes are being developed to comprise various chemotherapeutic agents together with surface functionalization to solve these problems [11,13].

Modifying liposome-mediated targeting of cell surface receptors can improve the accuracy of drug release, making it increasingly recognized as an effective strategy for improving the effectiveness of cancer treatment [14–16]. Various methods can be used in functionalized liposome-mediated targeted cancer therapy to provide different beneficial characteristics, including increasing the stability of encapsulation compounds and the selection of cancer cells [17–19]. As research

* Corresponding author.
** Corresponding author.
E-mail addresses: chenhan0903@163.com (H. Chen), liwei_dds@163.com (W. Li).
[1] The authors contributed equally.

https://doi.org/10.1016/j.mtbio.2024.101035
Received 29 November 2023; Received in revised form 29 February 2024; Accepted 19 March 2024
Available online 20 March 2024
2590-0064/© 2024 Published by Elsevier Ltd. This is an open access article under the CC BY-NC-ND license (http://creativecommons.org/licenses/by-nc-nd/4.0/).

exemplified by Grabowska et al., antibody-modified liposomes were much more efficiently internalized *in vitro* than non-antibody-modified liposomes, while the extent and the pattern of *in vivo* tumor accumulation of both liposomes were identical [20]. Zhou and co-workers designed a lipid-peptide liposome to prevent premature drug release from liposomes by incorporating a zipper peptide into the lipid bilayer [21]. However, the on-demand release of drugs from the lipid-layer gap will still limit their therapeutic utility.

The emergence of stimuli-responsive nanocarriers solves the problem of uncontrollable drug release [22–25]. Among these nanocarriers, stimuli-responsive liposomes were usually developed to improve the release of the drug in target areas and thereby enhance the therapeutic effect *in vivo* [26,27]. Thermosensitive liposomes (TSL) in combination with focused mild hyperthermia (41–43 °C) have been widely investigated with promising results in pre-clinical and clinical settings [28–30]. ThermoDox® is the first and only thermosensitive liposome formulation to reach clinical development and has also demonstrated promising activity for the treatment of chest wall recurrent breast cancer in Phase II clinical trial (NCT00826085) when combined with hyperthermia [31,32]. Compared to traditional clinical liposome Doxil, ThermoDox® is a lipid-based heat-activated formulation of doxorubicin that relies on externally applied energy to increase tissue temperature and efficiently trigger drug release [33]. However, ThermoDox® involves only a few mol% of monopalmitoyl phosphatidylcholine contained in the gel-phase dipalmitoyl phosphatidylcholine bilayer of TSL to increase the overall phase transition-induced permeability of the bilayer, leading the process of drug release in response to temperature is not consummate [33,34]. Moreover, all ThermoDox®-based TSLs were designed based on the T_g (glass transition temperature) of phospholipids themselves, and thus, further optimization of thermosensitive mechanisms and effects remains a challenge [31,33,34].

Inspired by Okano et al.'s works on drug release and related carriers [22,25,35], we proposed the theory of thermosensitive passive targeting nanocarriers in our previous studies [36–41]. In these works, the *in vitro/vivo* performance and shape of particles could be improved by regulating microstructural parameters like the surface chain density ($\rho_{\text{surface chain}}$), which was proposed and defined by us as shown in the following equation [39]:

$$\rho_{\text{surface chain}} = S_{shell}/N_{agg} \tag{1}$$

where the S_{shell} and N_{agg} are the total surface area of a given particle and the total chain number inside the particle. Moreover, parameters such as R_{core} can further optimize the microstructure of the formulation.

$$R_{core} = \sqrt[3]{\frac{3N_{agg}N_{BMA}M_W}{4\pi\rho N_A}} \tag{2}$$

where N_{agg}, M_W, R, and N_A are the polymer aggregation number of block copolymers for each micelle, the molecular weight, the density at the bulk state (approximately 1 mg/mL), and the avogadro constant, respectively. Moreover, the microstructure strongly affected in *vitro/vivo* drug release when drug molecules diffuse out. The effects of the microstructure of nanoparticles on the drug diffusion efficiency (D) were also carefully studied and illustrated in another of our works [35,42]. The equation describing drug release was shown as follows [35]:

$$D_{drug} = D_0\left(1 - r/\zeta\right)^{e^{(-1/n-1)}} \tag{3}$$

where D_0, r, ζ, and n are the diffusion coefficient of the drug in solution, the size of the drug molecule, the mesh size between two crosslinking points or entanglement points, and a constant. The D was dominated by the mesh size (ζ) inside the particle, which could be further regulated in the preparation process. As a result, based on the above research foundation, parameters such as $\rho_{\text{surface chain}}$, R_{core}, and ζ can be regulated to achieve its thermosensitive passive targeting function and more efficient drug release.

In this work, we endeavor to develop an active-to-passive targeting therapeutic to TSL with core-shell thermo-response capability aimed at increasing the therapeutic index of doxorubicin. In the synthesis of dual-thermosensitive liposomes (DTSL), 09JA as a block copolymer can be inserted into the lipid layer to enhance the thermosensitive responsiveness of the DTSL, and K3 as a cluster copolymer can be the thermo-responsive core of the DTSL with a stable structure (Fig. 1A). 09JA and K3 were thermosensitive polymers prepared based on our previous studies [33–36]. With K3 as the core and 09JA in the lipid layer as the shell, DTSL (sample d) exhibits thermal responsiveness at 42 °C and circulatory stability. Then, surface modification of liposomes with HER-2 Fab made the liposome achieve specific binding onto cancer cells and subsequent internalization. Therefore, the higher temperature in the tumor microenvironment can trigger the binding of the phospholipid layer and cell membrane of DTSL-fab to achieve active passive dual targeting and sufficient drug release. *In vivo* experiments, we conducted the tissue distribution and tumor accumulation of DTSL-fab in comparison to nontargeted liposomes using the N87 xenograft tumor model and different synthetic schemes of liposomes. Moreover, our *in vivo* distribution investigations were also designed at 24 h after intravenous administration to trigger liposomal drug release after maximum tumor accumulation, and desirable improvement in the biological activity was observed from DTSL-fab compared to the conventional liposomes.

2. Materials and methods

2.1. Materials

1-palmitoyl-2-oleoyl-*sn*-glycero-3-phosphocholine (PC) and Mal-PEG-DSPE were purchased from Avanti. Thermosensitive copolymer 09JA and K3 were synthesized in our previous works [35,42,43]. Doxorubicin hydrochloride was purchased from Dalian Meilun. The dialysis-membrane was purchased from Spectrum. Cell Counting Kit-8 Test Kit was purchased from DOJINDO. Fetal Calf Serum, Dulbecco's modified Eagle's medium (DMEM) was purchased from GIBCO. Anti-HER-2-Fab provided by Zhangjiang Biotechnology. All chemicals are analytical grades and used as received. Milli-Q water (18 MΩ cm) was used for all solution preparations. All glassware was treated with freshly prepared aqua regia and was used after rinsing with water three times.

2.2. Synthesis of liposomes

0.5 mg K3, 0.5 mg 09JA, 0.25 mg Mal-PEG-DSPE, and 2.0 mg PC were mixed in the methanol and chloroform intermixture (volume ratio = 1:1), then take the mixture in the 50 mL evaporator with nitrogen protection in rotary evaporators for 5 min (50 r/min) Fig. S1. Dissolve 6 mg DOX in the PBS to 3 mL, then use the mixture elute the flask in the protection from light, then dialysis with MilliQ-water (MWCO 3.5 KD) for 24 h.

2.3. Preparation of single fab fragment

As shown in Fig. 1A iii, the anti-HER-2-Fab fragment from the anti-HER-2 monoclonal antibody (mAbs) was prepared by our group as reported previously [43]. 10 mg/mL anti-HER-2 mAb (0.1 M acetate buffer, pH = 4.5) was incubated with 0.25 mg/mL de pepsin at 37 °C overnight followed by centrifugation and dialysis against TBS (145 mM NaCl and 10 mM Tris, pH = 7.5) for 18 h. The Staph A-Sepharose column (Pharmacia) was used to remove the undigested mAbs at pH = 8.0, then purified by the Sephadex G-150 column (Pharmacia) which was pre-equilibrated by the buffer 1 (0.1 M NaCl, 0.1 M borate, 0.05 M citrate, and 2 mM EDTA, pH = 5.5). Such solution was concentrated at 10 mg/mL and was further digested by the enzyme papain. The fab fragment solution was purified by the same procedure as mentioned above

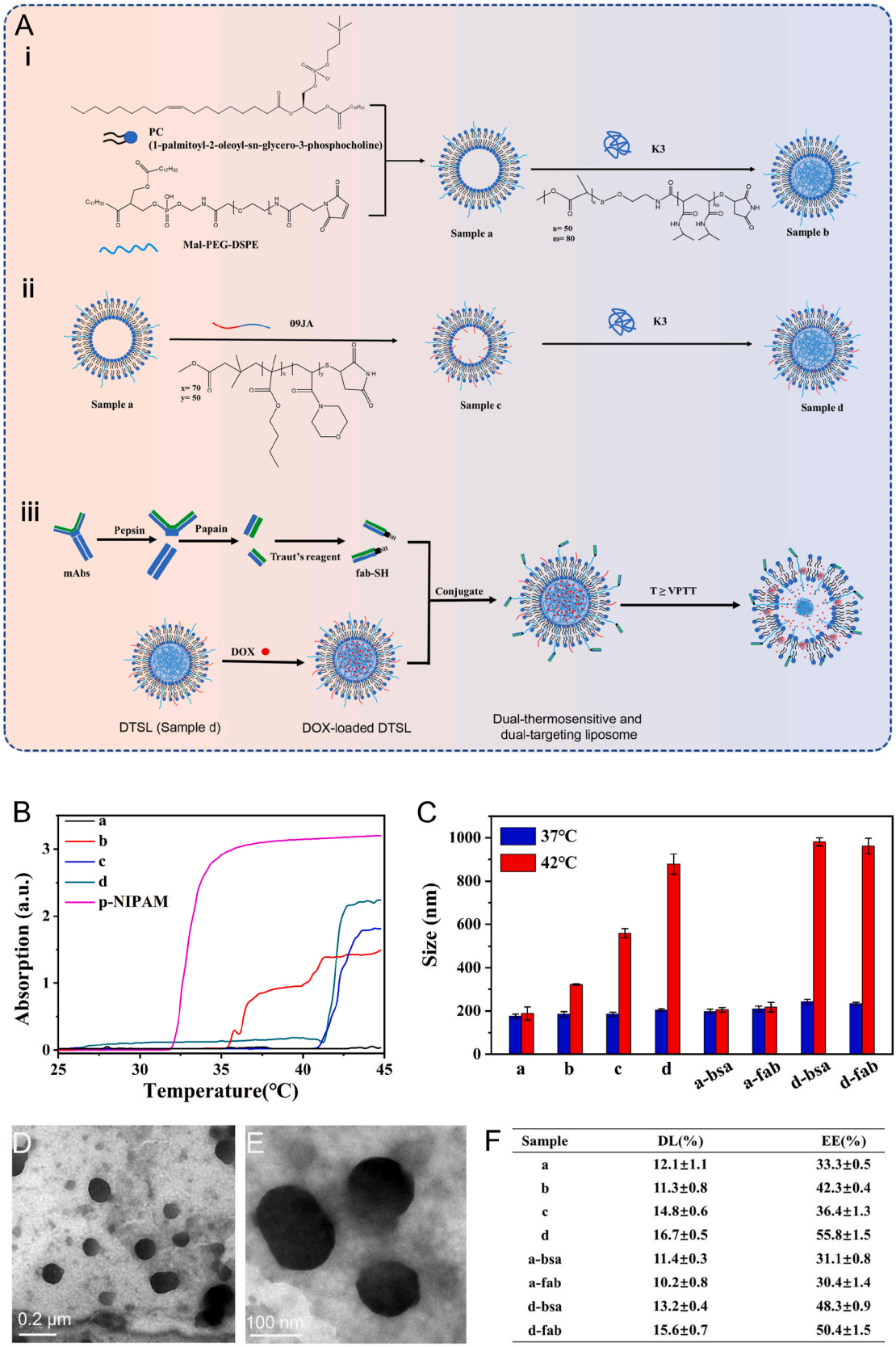

F

Sample	DL(%)	EE(%)
a	12.1±1.1	33.3±0.5
b	11.3±0.8	42.3±0.4
c	14.8±0.6	36.4±1.3
d	16.7±0.5	55.8±1.5
a-bsa	11.4±0.3	31.1±0.8
a-fab	10.2±0.8	30.4±1.4
d-bsa	13.2±0.4	48.3±0.9
d-fab	15.6±0.7	50.4±1.5

Fig. 1. A: Design of the liposomes. i: Synthesis of liposome a (PC + Mal-PEG-DSPE), b (PC + Mal-PEG-DSPE + K3). ii: Synthesis of liposome c (PC + Mal-PEG-DSPE+09JA) and d (PC + Mal-PEG-DSPE + K3+09JA). iii: Schematic of Anti-HER-2-Fab modified liposome and presentation of drug release when T ≥ VPTT. B: VPTT of liposome a, b, c, d, and *p*-NIPAM at temperatures from 25 °C to 45 °C. C: Size of the different liposomes (a, b, c, and d) with BSA (a-bsa and d-bsa) and FAB modified (a-fab and d-fab) at 37 °C and 42 °C (n = 3). D and E: TEM of liposomes at room temperature (liposome d). F: Drug loading and encapsulation efficiency of different liposomes.

resulting in a single fab fragment.

2.4. Preparation of bsa-SH and fab-SH

1 mg bovine serum albumin (bsa) or anti-HER-2 mAb (fab) fragment was mixed in PBS solution with 0.075 mg 2-IT (2-iminothiolane. HCl), then reacted at room temperature of 25 °C and shaker rate 60 rpm for 2 h. Then take the solution in Dialysis-membrane (MWCO 1 KD) dialysis with the 50 mM HEPES (pH = 7.4) for 24 h. The solution of bsa-SH and fab-SH was stored at 4 °C and N_2 environment for future use.

2.5. Synthesis of modified liposomes

The solution of bsa-SH and fab-SH mixed with liposomes a and d in the molecular ratio of Mal-PEG-DSPE in 1:10, incubation in the shaker under room temperature and N_2 for about 8 h. After incubation dialysis (MWCO 100 KD) in the PBS solution for 24 h in 4 °C exchange resulting in the a-bsa, a-fab, d-bsa, and d-fab.

2.6. Size distribution and morphology by DLS

The liposomes were dispersed in 0.2 M phosphate buffered solution (PBS, pH = 7.4). Such diluted liposome solution was filtrated by a hydrophilic membrane 0.45 μm Millipore filters. The hydrodynamic diameter and size distribution were determined by Dynamic Light Scattering CGS-3 (ALV, German) at 25 °C and 90° scattering angle.

2.7. Transmission electron microscopy (TEM) of thermosensitive liposome

The appearance examination of liposomes was conducted by transmission electron microscope (TEM). All samples were diluted with MilliQ-water and put on copper grids, which were air-dried and negative stained by 1% (w/v) sodium phosphotungstate ahead of the observation. To prepare stained specimens for the typical TEM (H-600A, Hitachi, Japan) experiments, about 5 μL liposome solution with a concentration of 2 mg/mL was dropped on 200-mesh formvar-free carbon-coated copper grids (Ted Pella Type-A; nominal carbon thickness 2–3 nm). After the water evaporated by exposing the sample to air at room temperature, the sample was inversely covered with a small drop of hydrodated phosphotungstate (PTA) solution with a mass fraction of 2%. The conventional TEM images were obtained at 100 kV.

2.8. Drug loading and encapsulation efficiency

DOX-loaded liposome (1 mL) was put in a dialysis membrane (MWCO 14 KD), which was immersed in 250 mL PBS (0.2 M, pH = 7.4) containing 0.1% (w/v) Tween 80 and kept at 37 °C and 100 rpm. At predetermined time intervals, aliquots of 1 mL were taken out and replaced with an equal volume of fresh-release medium. The amount of released DOX was analyzed by Fluorophotometer (Varian Eclipse). The drug loading and encapsulation efficiency were measured by UV at 480 nm and calculated by the following function:

$$\text{Drug loading } \% = \left(W_{\text{DOX inside liposome}} \,/\, W_{\text{Liposome}}\right) \times 100 \quad (4)$$

$$\text{Encapsulation efficiency } \% = \left(W_{\text{DOX inside liposome}} \,/\, W_{\text{DOX}}\right) \times 100 \quad (5)$$

2.9. In vitro DOX releasing profile

A dialysis bag (MWCO 3.5 KD) containing about 3.0 mL DOX-loading liposomes solution was put in a beaker with 500 mL MillQ-water tuned by Dulbecco's phosphate-buffered saline (PBS) at pH 7.4. The beaker was fixed in a water bath kept at 37 °C and 42 °C with continuous siring. The initial DOX concentration in the liposome is about 0.5 mg/mL. The DOX-loading liposomes mixture was continued to be dialyzed with the PBS buffer solution. About 0.5 mL PBS solution outside the dialysis bag was sampled at specific time intervals and analyzed by UV to determine the accumulated drug release profile.

2.10. Cell culture

The human stomach cancer cell N87 which overexpressed HER-2 antigen, cultured in the medium: Dulbecco's modified Eagle's medium (DMEM) supplied with 10% fetal bovine serum (FBS), 50 unit/mL penicillin, and 50 mg/mL streptomycin at 37 °C with 5% CO_2. Before all the cell line experiments, the cells were pre-cultured overnight until confluence reached 75%.

2.11. Cytotoxicity

N87 cells were seeded in 96-well plates at a density of 5000 cells per well and cultured for 12 h in a cell incubator (7% CO_2, 37 °C or 42 °C). Then incubated two 96-well plates with all samples (a, b, c, d, a-bsa, a-fab, d-bsa, and d-fab) at DOX equivalent doses of 1, 2, 3, 4, 5, 6, 8, and 10 μg/mL, then one plate was take in the cell incubator (7% CO_2, 37 °C) for 24 h and the other one was take in the 42 °C incubation for 12 h and then take into the 37 °C cell incubator for 12 h. Cell Counting Kit-8 (CCK-8) assay was used to determine cell viability. Untreated cells served as 100% cell viability. The absorption of the samples in each well was measured by the microplate reader with a wavelength of 480 nm. The percentage of surviving cells was calculated according to the following equation [36]:

$$\text{Surviving cells } (\%) = \left(A_{\text{sample}} - A_{\text{blank}}\right) / \left(A_{\text{control}} - A_{\text{blank}}\right) \times 100 \quad (6)$$

Where the A_{sample}, A_{blank}, and $A_{control}$ are UV absorption at 450 nm from cells incubated with liposomes, the culture medium, and the cell without liposomes.

2.12. Cellular uptake by flow cytometer and fluorescent microscopy

Cellular uptake and internalization by flow cytometer and fluorescent microscopy N87 cells were seeded into a 24-well microplate (0.5 mL/well, 2×10^5 cells/mL) and cultured for about overnight till the cells reached 60% confluence. Then, N87 cells were incubated with free DOX, non-modified liposomes (a, b, c, and d), and modified liposomes (a-bsa, a-fab, d-bsa, and d-fab) solutions at 37 °C and 42 °C for about 12 h and 24 h. Then the N87s were gently rinsed with DMEM/FBS twice. Trypsin to digest the cell for about 2 min and then rinsed by PBS and centrifuged twice with 800 rpm for 5 min. Finally, the flow cytometry and Fluro View FV1000 (Olympus) microscope were used to check the fluorescence intensity of DOX, non-modified liposomes (a, b, c, and d), and modified liposomes (a-bsa, a-fab, d-bsa, and d-fab).

2.13. Tumor accumulation and tissue distribution of liposomes in vivo mediated

The experimental animals (Balb/c nude mice, female, 4–6 weeks, ~20 g) were purchased from the Shanghai Experimental Animal Center of Chinese Academic of Sciences (Shanghai, P. R. China). Balb/c nude mice were maintained in a pathogen-free environment and allowed to acclimate for at least one week before tumor implantation. All studies were performed according to the guidelines of the Committee on Animals of Naval Medical University, Shanghai, PR China. The tumors model was induced in the right backside space of 4–5 weeks female nude mouse by subcutaneous injection of 0.1 mL (5×10^7 cells per 1 mL) of human gastric carcinoma cells N87.

In the study of *in vivo* distribution, mice bearing N87 tumors were randomly assigned to 10 groups with 2~3 mice/group. When the tumor size reached approximately 60 mm^3, targeting and non-targeting liposomes (bsa modified liposomes, fab modified liposomes) loading fluorescein isothiocyanate (FITC) with equivalent to 5 mg/kg dosage were

administered *via* tail vein. At the 12 h and 24 h points after injection, the mice were anesthetized by 1.5% isoflurane in 1:2 O_2/N_2. The *in vivo* images were observed with an IVIS® imaging system (excitation 500 nm) and recorded by a built-in CCD camera. Mice were sacrificed at the point of 12 h and 24 h, then excised heart, liver, tumor, spleen, and kidney. These organs were also imaged with the same excitation wavelength. Then the organs were collected and immediately fixed in formalin for 1 h. The organs were frozen in tissue Tek-OCT and cryosections. Frozen sections were cut at 10 mm sections and fixed with acetone. After washing with PBS, sections were counterstained with 4',6-Diamidino-2-phenylindole dihydrochloride (DAPI, Sigma, Fluka Chemie, Buchs, Israel) and visualized by inverse fluorescent microscopy.

When the tumor size reached approximately 60 mm^3, the mice were randomly assigned to six groups with 6 mice/group and injected intravenously through the tail vein with DOX injection, all samples (the control, free DOX, a-bsa, a-fab, d-bsa, and d-fab) at an equivalent DOX dose of 5 mg/kg. Tumor size was recorded every 2 days by a digital vernier caliper. The tumor volume (V) was calculated according to the following equation:

$$V_{tumor} = L \times W^2/2 \quad (7)$$

where L and W were the longest and shortest diameters. Tumor progression was evaluated in terms of relative tumor volume (to day 0) over 15 days.

2.14. Statistical analysis

All experimental data were presented as means ± SD. P-values were calculated using the student's t-test between two groups or one-way Analysis of Variance (ANOVA) followed by post-hoc Tukey analysis among three or more groups. For normally distributed data, the Mann-Whitney rank sum test was used. The differences were judged to be significant at $p < 0.05$.

3. Results

3.1. Preparation and characterization of liposome

Four kinds of liposomes (a, b, c, and d) with different ratios of thermosensitive copolymer 09 JA and K3 were synthesized in this study. As shown in Fig. 1A, the copolymer K3 as the core, and 09JA as the shell through grafting polymerization Mal-PEG-DSPE, onto PC, which could self-assemble as liposomes. Specifically, a liposome containing only phosphatidylcholine (PC) and Mal-PEG-DSPE is named liposome a. Liposome b is prepared with a thermosensitive polymer K3 as the core and liposome a as the outer shell, which is a core thermosensitive TSL. Liposome c is prepared by inserting the other thermosensitive polymer 09JA into the liposome, which is a shell thermosensitive liposome. Combining with the above synthetic step of different TSL, dual-thermosensitive liposomes (DTSL, sample d) are prepared by encapsulating K3 as the core and inserting 09JA in the lipid layer as the shell. Subsequently, anti-HER-2 Fab fragments were conjugated to the distal ends of PEG chains in these liposomes to achieve better tumor-targeting performance. Furthermore, according to the design, mild hyperthermia of tumor microenvironment triggered doxorubicin release from optimized thermosensitive liposomes improves intertumoral drug delivery and efficacy of the tumor.

To verify the Volume Phase Transition Temperature (VPTT) of liposomes, UV–vis absorption spectra were scanned with *p*-NIPAM as control. As shown in Fig. 1B, the VPTT of liposome b, c, and d were 36 °C, 41 °C, and 42 °C, respectively. As controlled samples, the VPTT of *p*-NIPAM was 33 °C, and liposome d presented no VPTT. The particle size and thermo-responsiveness of the liposome were optimized by modulating the proportion of 09 JA and K3. In detail, the average hydrodynamic diameters of liposome a-bsa, a-fab, d-bsa, and d-fab were 189.12 ± 16.20 nm, 191.69 ± 20.16 nm, 224.50 ± 14.33 nm, and 234.71 ± 18.11 nm at 37 °C, respectively (Fig. 1C). The liposome a-bsa, a-fab, d-bsa, and d-fab were also put into 42 °C water bath, and then determine the average hydrodynamic diameters (Fig. 1C). Compared to sample a-bsa and a-fab, d-bsa and d-fab showed an obvious size change after the temperature increase to 42 °C. As a result, liposome a and d were selected as the liposome modified with bovine serum albumin (-bsa) and HER-2 antibody (-fab). To further verify the stability of the drug-loading liposomes, place the sample at room temperature for observation within 96 h, liposome c and d showed a stable condition, while as controlled samples, liposome a and b presented sediment at the bottom (Fig. S1). The liposome c and d experienced the most obvious alteration in size and even precipitated when the temperature increased from 37 °C to 42 °C on dialysis (Fig. S2).

Furthermore, TEM images displayed that the liposome is a "bulb" in shape with loosely extending chains surrounded at room temperature, which were consistent with the alteration in size (Fig. 1D). The successful encapsulation of DOX in the liposome was further confirmed by UV–vis absorption measurements. Specifically, as listed in (Fig. 1E), the drug loading (DL) and encapsulating efficiency (DL) of liposome a, b, c, and d were 12.1%, 11.3%, 14.8%, 16.7% and 33.3%, 42.3%, 36.4%, 55.8%, respectively. With bovine serum albumin (-bsa) and HER-2 antibody (-fab) modified, the DL and EE of liposome a-bsa, a-fab, d-bsa, and d-fab were 11.4%, 10.2%, 13.2%, 15.6% and 31.1%, 30.4%, 48.3%, 50.4%, respectively.

3.2. In vitro releasing profile

The thermal responsiveness of DOX-loading liposome was studied by quantifying the amount of encapsulated drug release at 37 °C and 42 °C, respectively. As shown in Fig.2Ai-iv, compared to DOX, the suspension exhibited a rapid increase in drug release with time and eventually reached a plateau, and no significant leakage of DOX from sample a, b, c, and d was observed after incubation for 60 min at 37 °C. The release of free DOX molecules was examined as a control group, which showed a complete cumulative release within 12 h. To verify temperature responsiveness release of the liposomes in parallel at 42 °C, as shown in Fig. 2A ii, the releases of liposome c and d were potentiated at 42 °C and evident thermo-triggered burst release of DOX. By contrast, liposome a and b exhibited no burst releases at 42 °C. As displayed in Fig. 2A iii and Fig. 2A iv, liposomes modified of bsa and HER-2-fab, d-bsa, and d-fab presented a faster drug release at 42 °C condition compared to a-bsa and a-fab. Observed by further analysis of median release time (Fig. 2B) and halftime cumulate release (Fig. 2C), liposome d showed the desired temperature-dependent drug release property with much faster drug release than liposome a.

3.3. In vitro cytotoxicity and cellular uptake

To further evaluate the *in vitro* cytotoxicity of a, b, c, d, a-bsa, a-fab, d-bsa, and d-fab, cell viability in N87 cell lines was measured using Cell Count Kit-8 (CCK-8) under incubation conditions of 37 °C. Compared with other drug-loaded liposomes, d-fab exhibited the lowest cell viability after incubation at different temperatures (Fig. 3A–D). Moreover, to evaluate the bioavailability and cytotoxicity of liposomes in the tumor microenvironment, cells were treated under incubation conditions at 42 °C. Similarly, the cytotoxic effect observed was dependent on anti-HER-2-fab antibody conjugation to liposomes, and concretely, a-fab and d-fab showed significantly lower cell viability, compared to a-bsa and d-bsa. Meanwhile, sample d, d-bsa, and d-fab showed enhanced cytotoxicity at 42 °C incubation conditions compared to incubation conditions of 37 °C and even approached free DOX cytotoxicity at identical DOX concentrations. In comparison, free DOX presented the highest cytotoxic activity on N87 cells because of the rapid uptake of the drug by the cells in its free form.

The cellular uptake of the liposomes and their internalization into

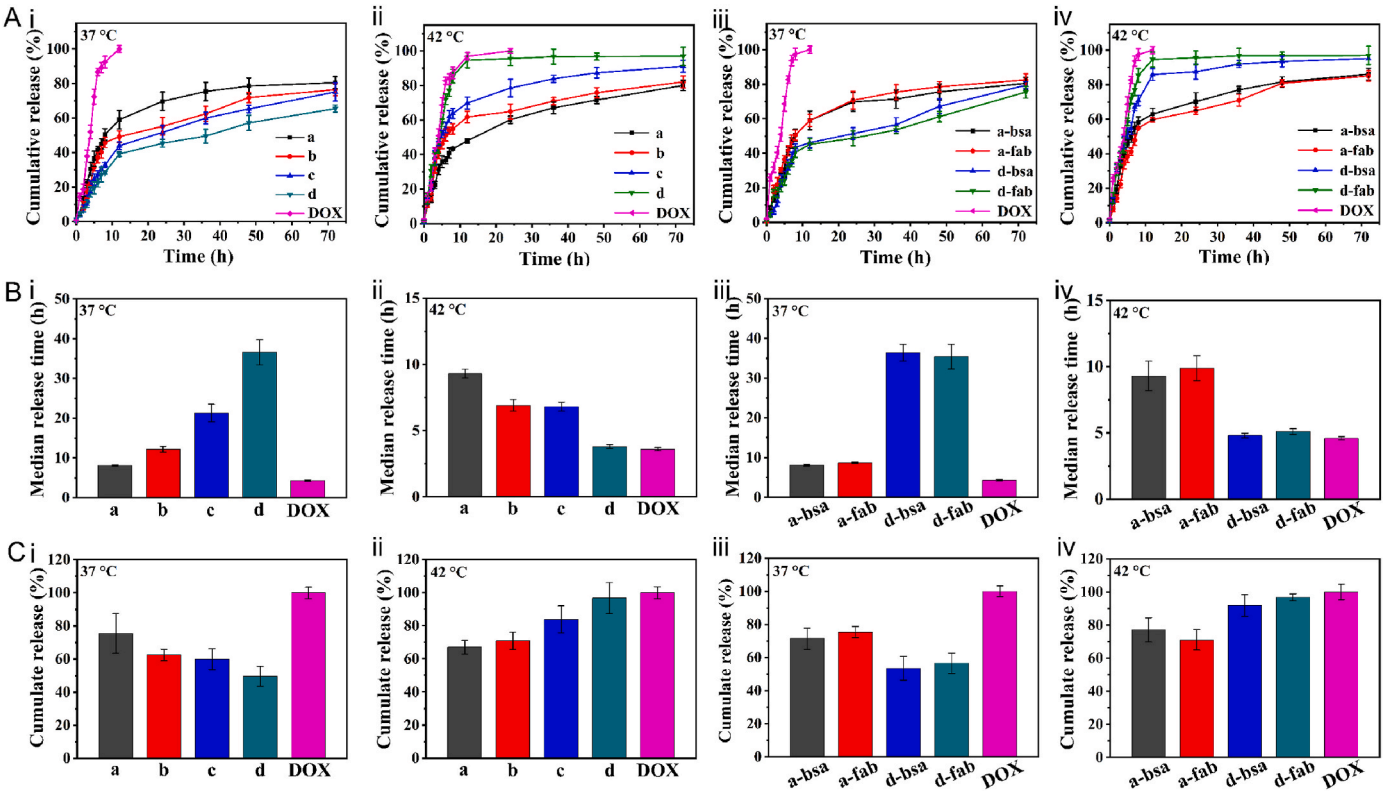

Fig. 2. A: DOX release from liposomes (sample a, b, c, and d) and modified liposomes (sample a-bsa, a-fab, d-bsa, and d-fab) after incubation at 37 °C (i and iii) and 42 °C (ii and iv). B: Median release time of liposomes (sample a, b, c, and d) and modified liposomes (sample a-bsa, a-fab, d-bsa, and d-fab) after incubation at 37 °C (i and iii) and 42 °C (ii and iv). C: Cumulation release of DOX from liposomes (sample a, b, c, and d) and modified liposomes (sample a-bsa, a-fab, d-bsa, and d-fab) after incubation at 37 °C (i and iii) and 42 °C (ii and iv) for 36 h (half time of total release time). DOX release experiments were performed in a phosphate buffer solution to simulate physiological conditions. Data are presented as mean ± SD (n = 3).

N87 cells was studied next by flow cytometry (FCM) (Fig. 3E–H). The cellular uptake of the encapsulated drug (DOX) after 12 h and 24 h incubation with cells was enhanced by the HER-2-fab and the condition of 42 °C. Rapid binding and internalization of DOX from sample c and d into N87 cells was observed as early as 12 h after incubation at 42 °C conditions, which increased further over 24 h. In comparison, only moderate cellular uptake was observed from sample a and b after 12 h incubation, presumably through non-specific endocytosis, which also increased further over 24 h.

Less internalization of a-bsa and d-bsa was observed based on DOX fluorescence by fluorescence microscopy, further indicating the poor levels of cellular uptake compared to a-fab and d-fab (amount of DOX internalized close to background levels) (Fig. 3I and Fig. S3). The results of fluorescence microscopy also demonstrated slightly lower cellular uptake of DOX in the case of all liposomes compared to free DOX within 24 h of incubation at 37 °C, while at 42 °C, the significantly enhanced the DOX cellular uptake of liposome d, d-bsa, and d-fab indicated by the increased red fluorescence intensity. However, cellular uptake of sample a, a-bsa, and a-fab showed no difference at 37 °C and 42 °C. These data agreed with the cellular uptake findings above and indicated that although some spontaneous release of DOX could occur after HER-2-fab modification, the intracellular bioavailability, triggering the release of DOX at 42 °C can significantly improve the intracellular bioavailability of drug molecules, thereby enhancing their activity.

Different conditions of temperature will influence the way d-fab acts with cells. To verify this, each group was incubated with d-fab and DOX under conditions with temperature changes to observe their endocytosis, uptake, and cell viability. Fig. 4A showed the fluorescence microscope images of each group of d-fab and DOX after incubation for 12 h and 24 h under different conditions (42/37: incubate at 42 °C for 12 h then incubate at 37 °C for 12 h; 37/42: incubate at 37 °C for 12 h then incubate at 42 °C for 12 h). As shown in Fig. 4A, red fluorescent clusters (indicated by white arrows) appeared around the cells in the d-fab 42/37 group at 12 h, and they were not swallowed by the cells. After returning to 37 °C at 24 h, d-fab 42/37 showed strong intracellular fluorescence, which was caused by the entry of DOX into the cell after the release of DOX. But d-fab 42/37 also still has large red fluorescent clusters the same as at 12 h. Compared with the d-fab 42/37 group, the d-fab 37/42 group presented stronger DOX fluorescence (indicated by yellow arrows) in the cells after 24 h, indicating that d-fab will be easier to enter cells and release DOX. As controlled samples, there was no difference in the DOX groups with the two treatments. Then further investigate the cell distribution, as shown in Fig. 4B–a mass of fluorescent clusters appeared outside the cells in the d-fab 42/37 group. In contrast, the red fluorescence in the d-fab 37/42 group appeared inside the cells (cell profile as indicated by white dotted lines). As shown in Fig. 4C, the intracellular uptake of the d-fab 37/42 is the highest, which is significantly higher than that of the d-fab 42/37 group by flow cytometry. The measurement results of cell viability also showed that under the same concentration conditions, the cytotoxicity of the d-fab 37/42 group was stronger than that of the d-fab 42/37 group (Fig. 4D), which was consistent with the results of cell fluorescence microscopy and cell uptake.

Therefore, these results provide important insights into cell uptake of active-to-passive dual targeting liposomes, and the schematic of liposomes interaction with the cell is shown in Fig. 5A. Firstly, the HER-2-fab antibody on the surface of liposomes binds with the receptor on the cytomembrane (Fig.5Ai). After that, with the temperature increase of incubation, 09JA changes from linear agglomeration to cluster, and the gaps of the lipid layer enlarge with drug release (Fig.5Aii). Then, the lipid molecules of liposome and cytomembrane fuse. Finally, the endosomes endocytosis the liposomes into the cell with lipid insertion (Fig. 5

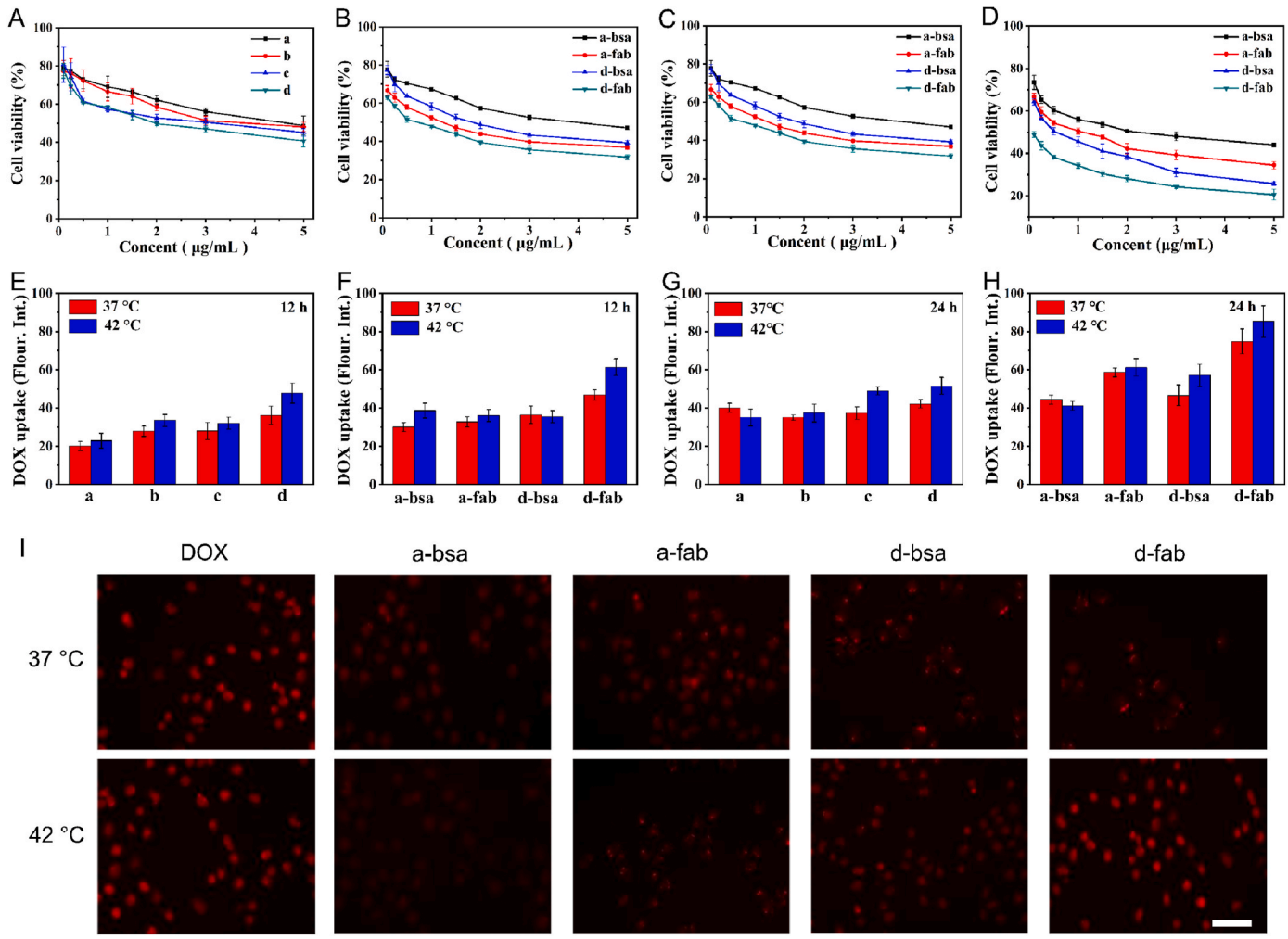

Fig. 3. Cell viability of liposome (a, b, c, d, a-bsa, a-fab, d-bsa, and d-fab) at 37 °C (A and B) and 42 °C condition (C and D). Cell uptake of liposome (a, b, c, d, a-bsa, a-fab, d-bsa, and d-fab) at conditions of 37 °C and 42 °C after incubation for 12 h (E and F) and 24 h (G and H). I: Fluorescence microscope image of liposome (a-bsa, a-fab, d-bsa, and d-fab) at conditions of 37 °C and 42 °C after incubation for 24 h. The scale bar represented 50 μm. Data are presented as mean ± SD (n = 5).

A iii). To verify this phenomenon, we investigated the release of the liposomes at different temperatures (27 °C, 37 °C, 40 °C, 41 °C, and 42 °C). The release amount of liposome a did not change at different temperatures, while the release amount of liposome d increased with the increase in temperature, reaching the highest half-release amount and the shortest half-release time at 42 °C (Fig. 5B and C).

3.4. *In vivo distribution*

The therapeutic efficacy of targeted liposomes will depend not only on their cell receptor binding and internalization but also on their ability to travel deeper within the tumor interstitium [16–19]. To evaluate the *in vivo* distribution of liposomes, fluorescein FITC instead of DOX was encapsulated into different nano-formulations. *In vivo* distribution analysis of FITC encapsulated nanocomposites was performed in tumor-bearing Balb/c nude mice. In agreement with FITC tissue distribution, IVIS® imaging displayed that a-fab and d-fab were associated with higher DOX signals throughout the body. This was more obvious with the fab-modified compared to the bsa-modified. The liposome a-fab and d-fab showed better cellular uptake and cytotoxic activity compared to a-bsa and d-bsa, therefore this system was selected for further studies using *in vivo* distribution. To further validate the tissue distribution data, a-bsa, a-fab, d-bsa, and d-fab were followed by whole-body optical imaging of FITC fluorescence 12 h and 24 h after injection using an IVIS® camera (Fig. 6 A, B and Fig. S4).

Fig. 6 A, B, and Fig. S4 demonstrated that free FITC was almost cleared from the blood circulation at 12 h post-administration, the liposomes significantly extended the circulation time of encapsulated FITC. Moreover, different frozen sections of fluorescent images of bsa and fab modified samples demonstrated that the fluorescence in the kidney, spleen, liver, and heart was significantly reduced after BSA and fab-modified groups and free FITC injection groups. Besides, the tissue distribution of FITC was measured, and a higher fluorescence hepatic-accumulation of a-bsa, a-fab, and d-bsa compared to d-fab (Fig. 6C and Figs. S5 and S6). To obtain more accurate *in vivo* animal imaging results, the near-infrared fluorescent dye DIR was selected for fluorescence labeling of liposomes. As shown in Fig.6D, d-fab exhibited significantly higher tumor accumulation at different time points.

3.5. *In vivo antitumor activity*

The biodistribution data above indicated an increase in tumor uptake of the targeted liposomes compared to nontargeted liposomes. To evaluate the *in vivo* anti-tumor activities of saline (control), free DOX, a-bsa, a-fab, d-bsa, and d-fab, tumor-bearing mice were randomly administered tail vein injection of DOX. As shown in Fig. 7A and B, after the treatment, the tumor volume showed minimal growth and even a reduction in size within 15 days. It indicated that injection with a-bsa, a-fab, d-bsa, and d-fab loaded with DOX showed significant growth retardation compared to untreated animals. Besides, a-fab and d-fab

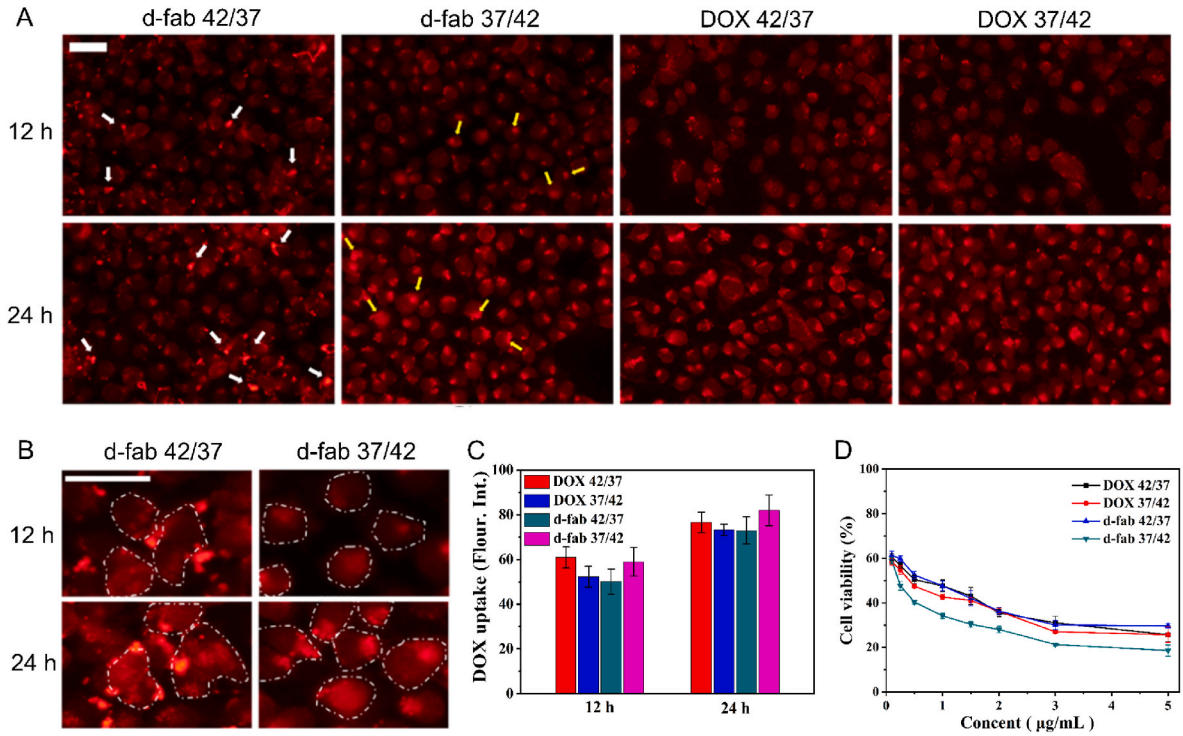

Fig. 4. (A) Fluorescence microscope image of cells with d-fab and DOX at different conditions (42/37: incubate at 42 °C for 12 h and then turn to 37 °C for 12 h; 37/42: incubate at 37 °C for 12 h and then turn to 42 °C for 12 h). The bar represents 20 μm. (B) Distribution of d-fab in cells with different incubate conditions. The bar represents 20 μm. Cell uptake (C) and cell viability (D) of d-fab and DOX with incubating conditions. Data are presented as mean ± SD (n = 3).

further decreased the tumor growth compared to a-bsa, d-bsa, and free drug groups. On day 13 and 15, the treatment groups a-fab and d-fab resulted in significant tumor growth retardation compared to the control group. Fig. 7A and Fig. S7A indicated that the tumor inhibition rates of DOX, a-bsa, a-fab, d-bsa, and d-fab were 73.7%, 76.2%, 83.1%, 81.1%, and 91.2% respectively. Tumor weights that were consistent with the tumor inhibition rate (Fig. S7B). Neither body weight loss nor apparent histological damage in mice treated with all liposomes was noted following the therapeutic course (Fig. 7C). To further examine *in vivo* antitumor activity, the single tumor growth curve of the different groups was shown in Fig. 7D and Fig. S8A, tumor growth was consistent in all groups and Fig. 7B. Histopathological section with Hematoxylin-eosin (H&E) staining examinations of tumor was observed by the tumor transection and fractionated, possessed prominent *in vivo* antitumor activity. As shown in Fig. 7E and Fig. S8B, the tumor reduction and cavitations appeared in the superficial tumor tissues after the tail vein injection of d-fab. Conversely, this phenomenon was not observed in control and DOX. All the histopathological sections of tissues illustrated all liposomes have high biocompatibility without tissue lesions (Fig. S9).

4. Discussion

Liposomes can enhance the localization of cytotoxic agents in some solid tumors and decrease drug uptake by sensitive organs [33–36]. Next-generation liposome systems are envisioned to possess active targeting and triggered drug-release capabilities [12–15]. The ability of antibody-targeted liposomes to be internalized by cells can result in improvements in drug bioavailability, especially for drugs acting against intracellular targets [15–17]. Similar moderate improvements in therapeutic efficacy have been observed previously by triggering intracellular release after tumor accumulation using HER-2-targeted TSLs [33]. However, the major obstacle to its clinical application stems from the lack of an ideal vector that could provide targeted drug delivery for drugs in tumors. To achieve this goal, A nanocomposite using the DTSL assembly strategy modified with HER-2 antibody is designed, which is integrated by multiple essential attributes, including sufficient extracellular stability, and active accumulation of drug release in tumors.

In this study, we successfully prepared sample a, b, c, and d. The thermo-responsive property of the fabricated shell of nanocomposite was obtained by incorporating K3 and 09JA synthesized based on NIPAM into the liposome. Sample c and d formed precipitation both with water bath at 42 °C (Fig. S1 and Fig. S2), that's due to the joining of polymer K3 and 09JA, which could conduct thermal conversion. In the different ratios of K3 and 09JA (Fig. 1A), the DTSL (sample d) with a thermosensitive polymer core-shell structure was selected as the liposome. Importantly, the gaps between vascular endothelial cells of leaky tumor vessels range from 100 nm to 2 μm in size, and therefore, all the liposomes could thus easily infiltrate into tumor tissues (Fig. 1B–D). The liposome d experienced dramatic changes in particle size when the temperature increased and could be changed into suspension by sonication (Fig. 2). This means that the stable spherical structure of the drug-loading liposomes was broken and could release drugs.

As illustrated in profiles of drug release, liposome a and b showed a slower drug release in 12 h, compared with those of liposome c and d, due to the more closely packed 09JA core. The liposome c and d resulted in slower drug release at 37 °C due to 09JA and K3-induced liposome contraction. Owing to the conformation change of the 09JA and K3, the drug releases of liposome c and d were significantly enhanced at 42 °C, and all these indicated that the incorporation of 09JA and K3 also had profound effects on drug release (Fig. 2A–C). In the release experiment, the release coefficient of sample b was without significant change after the temperature increased, which is consistent with the result of the particle size at 42 °C. This is largely due to the thermosensitive polymer K3 core of the liposome, which changes with the responsive structure after heating, but has no effect on the structure of the liposome and the release of the drug. Different from that of liposome b, liposome c showed a sudden release after temperature increases. This is probably because the thermosensitive polymer 09JA is embedded in the shell of TSL and changes its structure after the temperature rises, resulting in exposing the inner core to drug release. The thermosensitive polymer K3 and

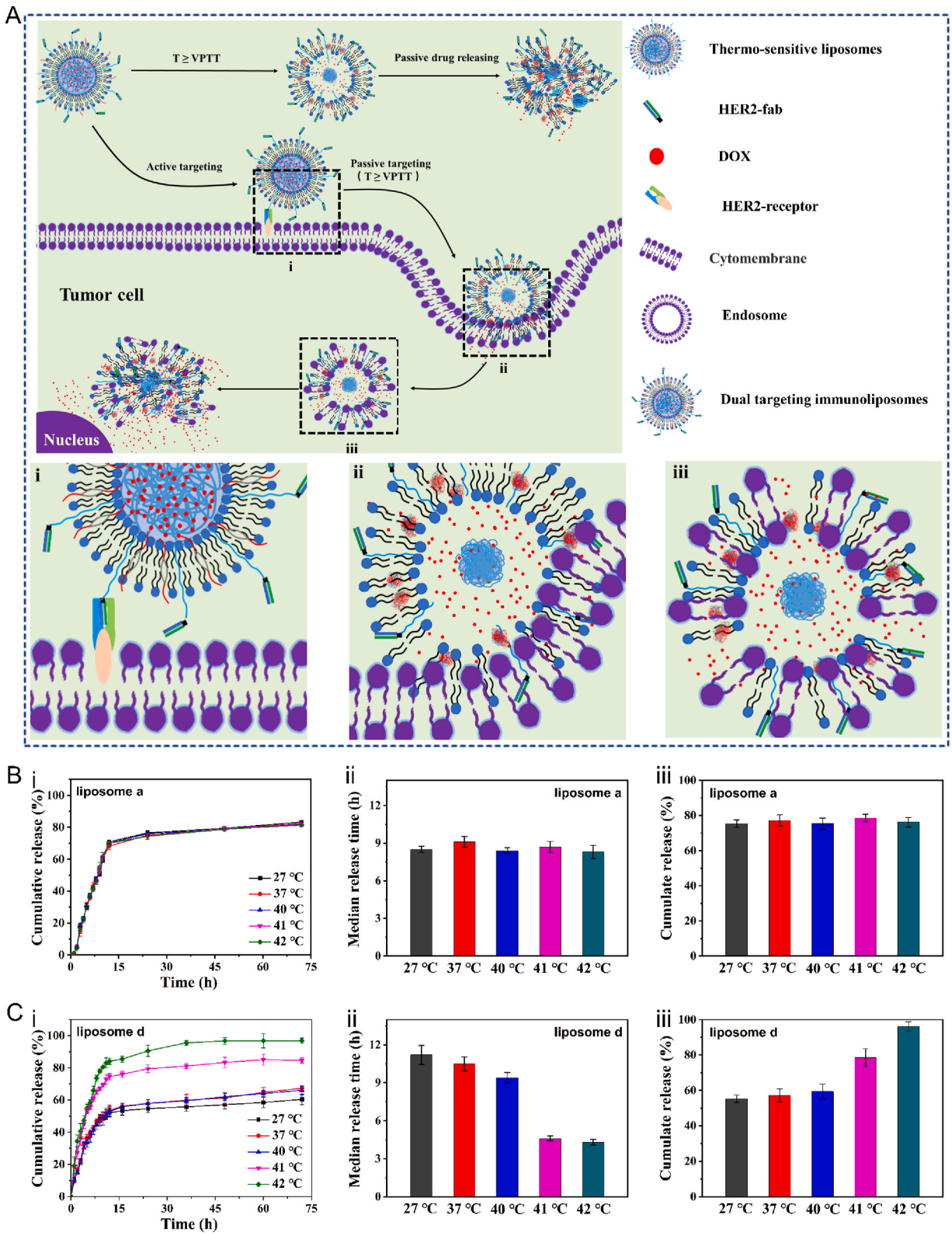

Fig. 5. A: Schematic of dual targeting liposomes interaction with cell. i: Antibody binding with the receptor on cytomembrane. ii: With the temperature increase, 09JA changes from linear agglomeration to cluster, and the gaps of the lipid layer enlarge with drug release, then the lipid molecules of liposome and cytomembrane fuse. iii: The endosomes endocytosis the liposomes into the cell with lipid insertion. B: i: DOX release from liposome a after incubation at 27 °C, 37 °C, 40 °C, 41 °C, and 42 °C. ii: Median release time of liposome a incubation at 27 °C, 37 °C, 40 °C, 41 °C, and 42 °C. iii: Cumulation release of DOX from liposomes a after incubation at27 °C, 37 °C, 40 °C, 41 °C, and 42 °C for 36 h (half time of total release time). C: i: DOX release from liposome d after incubation at 27 °C, 37 °C, 40 °C, 41 °C and 42 °C. ii: Median release time of liposome d incubation at 27 °C, 37 °C, 40 °C, 41 °C, and 42 °C. iii: Cumulation release of DOX from liposomes d after incubation at 27 °C, 37 °C, 40 °C, 41 °C, and 42 °C for 36 h (half time of total release time). DOX release experiments were performed in a phosphate buffer solution to simulate physiological conditions. Data are presented as mean ± SD (n = 3).

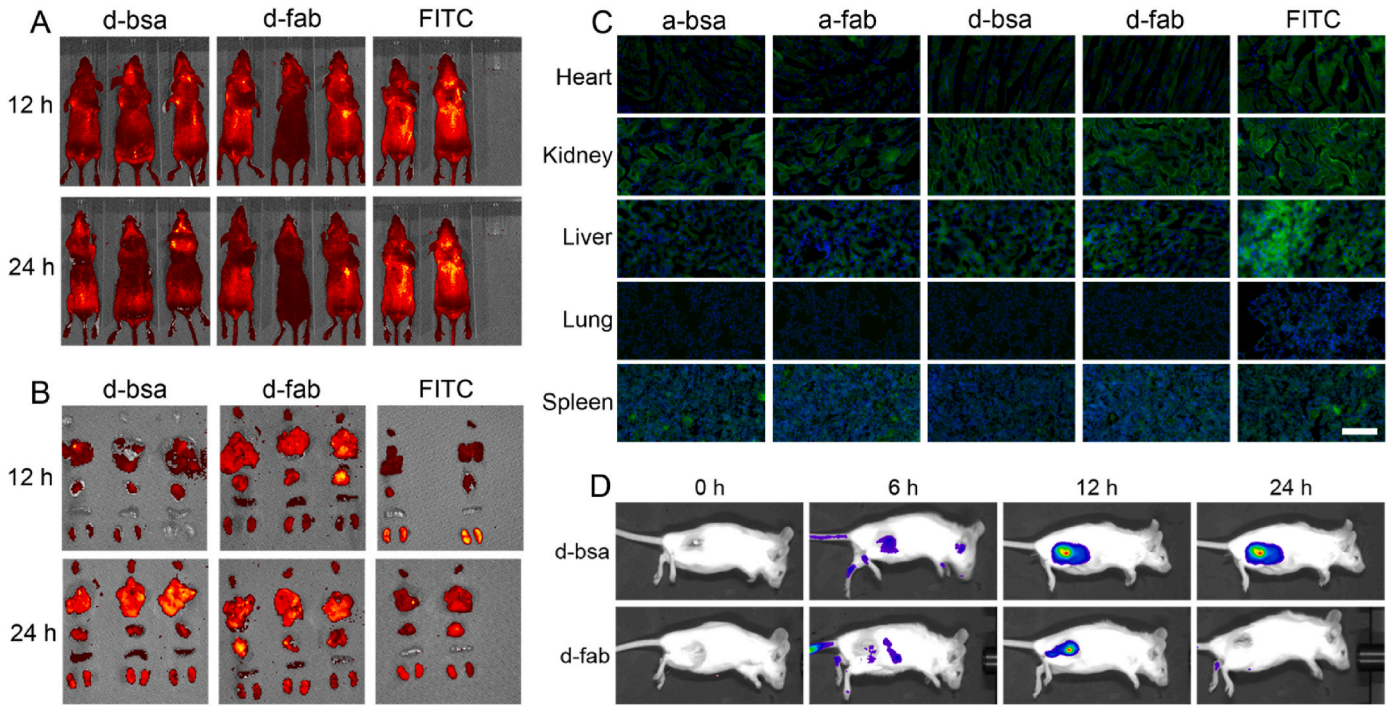

Fig. 6. *In vivo* distribution of a-fab, d-bsa, d-fab, and FITC. A: Whole-body imaging of athymic nude mice after injection with d-bsa, d-fab, and FITC for 12 h and 24 h (n = 3). B: Tissue imaging of athymic nude mice after injection with d-bsa, d-fab, and FITC for 12 h and 24 h. C: Confocal microscopy imaging of heart, kidney, liver, lung, and spleen within athymic nude mice after injection with a-bsa, a-fab, d-bsa, d-fab, and FITC for 12 h. The scale bar represented 200 μm. D: *In vivo* fluorescence images after intravenous injection of DIR-labeled d-bsa and d-fab into tumor-bearing mice at given time points.

09JA are simultaneously configured to change the shape of the carrier more quickly, thereby releasing the drug, as the liposome d.

For all the d-bsa and d-fab, the cell viability as incubated at 42 °C was lower than that at 37 °C due to the temperature promoting cell uptake and drug release as shown in the experimental results of cytotoxicity (Figs. 3 and 4). To verify the effect of this situation on active-to-passive dual-targeting liposomes, we investigated the uptake of liposomes to N87 cells by controlling the incubation conditions at different temperatures with time change. In this study, we measured the DOX uptake of cells under different conditions: 1) cell and liposome were incubated at 42 °C for 12 h and then placed at 37 °C and incubated for 12 h (42/37); 2) cell and liposomes were incubated at 37 °C for 12 h, then transferred to 42 °C for 8 h, and then incubated for 12 h (37/42). As shown in Fig. 4, the uptake of d-fab with condition 1 is significantly weaker than in condition 2, while a-fab, a-bsa, and d-bsa have no significant changes with the two treatments. To verify that the enhanced cytotoxicity is caused by endocytosis of d-fab at 37 °C, then incubation at 42 °C to release the drug in the cell, each group was observed by flow cytometry. Fig. 4D presented that the d-fab with condition 1 has the highest cellular uptake, which is consistent with cytotoxicity. Further observed by the fluorescent confocal microscope, the cell uptake of d-fab with condition 2 is stronger than that of the other groups, indicating that d-fab can be better taken up by cells in the first 12 h, and then released drugs in the cell, causing higher cytotoxicity. All these results indicated that the high temperature not only could promote the drug release from d but also facilitate cell endocytosis of the liposomes. This may be related to the modified HER-2-fab ability for endocytosis promotion. The peripheral antibody HER-2-fab of the liposome d is wandering around its periphery and is connected by long-chain Mal-PEG-DSPE (Fig. 5A). When the temperature increases, the outward pendulum Mal-PEG-DSPE is cross-linked with the inner core K3 and drags the fab and shrinks into the liposome shell. Then, the conformational change of the 09JA lipid shell further promotes the outward pendulum antibody embedded in the shell. Although this state enhances drug release in a passive targeting manner, as active-to-passive dual-targeting liposomes, this reduces its initial active targeting.

The longer circulation time can allow the liposomes to flow through and accumulate in the tumor site (Fig. 6). The tumor volume of d-fab showed a reduction in size with a whitish appearance, due to the disruption in blood vasculature (Fig. 7). Neither body weight loss nor apparent histological damage in mice treated with nanocomposites suggested that were potentially safe for *in vivo* application. The histopathological sections of tumor tissue showed that many cavities appeared in the superficial tumor tissues, attributed to the increasing accumulation of samples modified with HER-2-fab. Compared with free DOX, the tumor inhibitory effect of d-fab increased by 1.3 times, and the therapeutic effect was improved by using HER-2-fab modified liposomes to trigger intracellular release after tumor accumulation.

DOX-loaded DSTL (sample d-fab) have been successfully developed and studied thoroughly as cancer thermo-chemotherapeutics. The DSTL with HER-2-antibody modified (d-fab) maintain their physicochemical and structural integrity with stable retention of the drug and their thermal properties. These results have implications for other actively targeted drug delivery systems and can instruct on the challenges around the design of therapeutically efficacious multi-modal vesicle systems.

5. Conclusion

Our research indicates that DTSL with the core-shell structure of K3 and 09JA can effectively increase drug concentration in tumor cells and achieve a passive targeting mechanism. Moreover, active targeting of TSL d-fab is the main mechanism by targeting the tumor surface HER-2 receptors and then releasing drugs in cells. The active-to-passive dual-targeting TSL d-fab showed interesting and promising results like significant cell uptake *in vitro* and *in vivo*. While inlaying Mal-PEG-DSPE on the shell of TSLs might improve safety and circulation properties, we observed a decrease in liposome–cell interactions and drug delivery efficiency without antibody modification compared to free DOX *in vitro*. The dual-targeting DTSL d-fab significantly outperformed DTSL d-bsa in

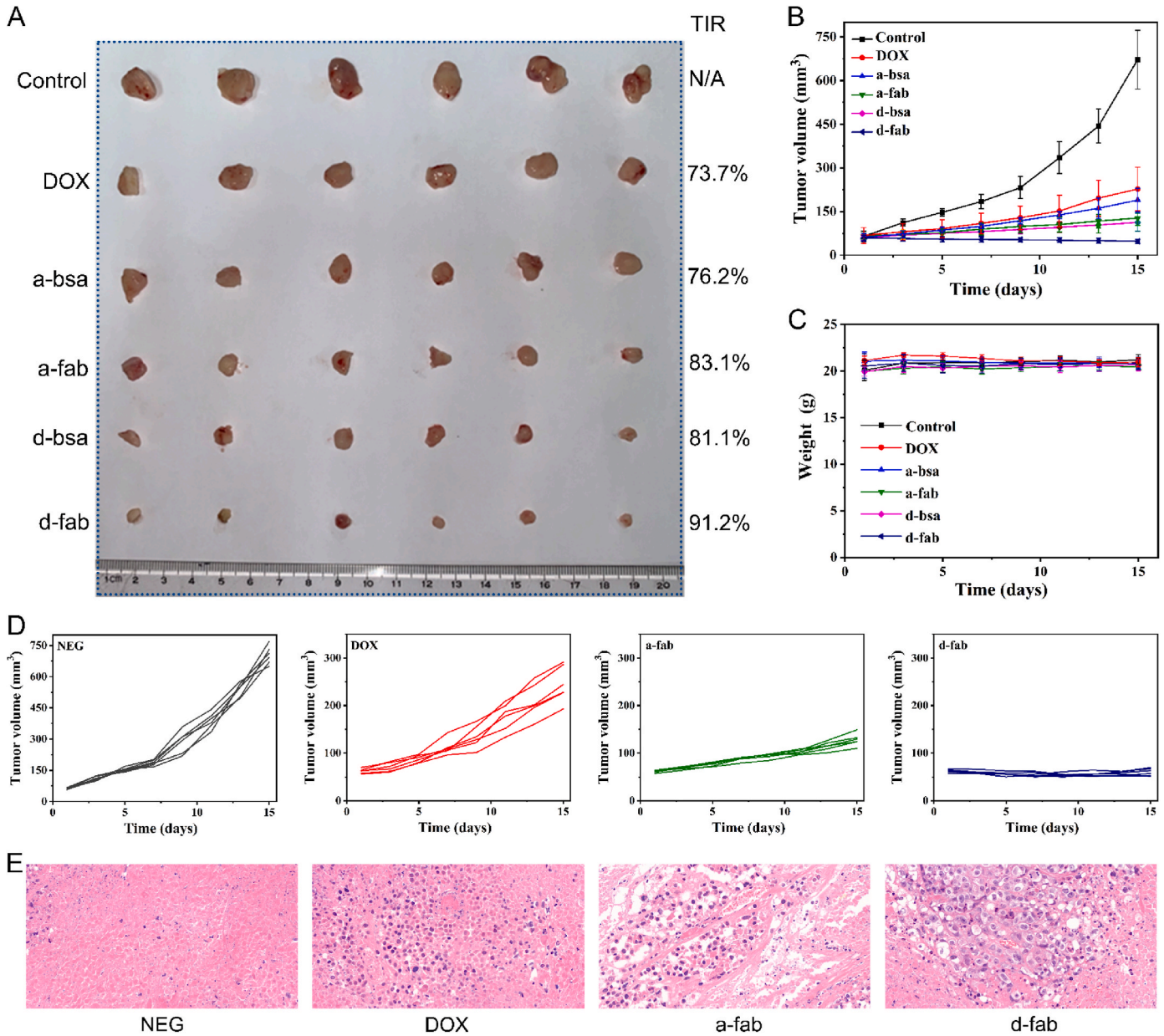

Fig. 7. *In vivo* tumor growth delay studies. N87 tumor-bearing mice were treated with liposomes applied after injection. A: N87 tumor-bearing mice treated with liposomes applied after injection. Tumor inhibition rate of saline (control), DOX, a-bsa, a-fab, d-bsa, and d-fab. B: Tumor volume *in vivo* after tail vein injection of saline (control), DOX, a-bsa, a-fab, d-bsa, and d-fab. C: Body weight following administration. D: The *in vivo* tumor growth curve. E: Hematoxylin-eosin (H&E) staining vertical section of tumor from groups saline (control), DOX, d-bsa, and d-fab. The scale bar represented 200 μm. A one-way ANOVA followed by Tukey's multiple comparison tests indicated significant tumor growth retardation in treated mice compared to control. Therapy started on day 11 after implantation with an average tumor size of 60 mm^3. Animals were injected intravenously with liposomes at 5 mg/kg DOX. Control animals were not injected. Data are presented as mean ± SD (n = 6).

terms of solid tumor targeting. All the experimental results demonstrated that the liposome could be an excellent drug delivery system for the treatment of tumors, which merits further investigation for preclinical experiments and clinical trials.

Ethics approval and consent to participate

All animal experiments were performed by the guideline of the Committee on Animals of Naval Medical University, Shanghai, PR China.

CRediT authorship contribution statement

Mengxin Zhao: Visualization, Validation, Software, Methodology, Investigation, Formal analysis, Data curation, Conceptualization. **Xiaodong Zhu:** Writing – review & editing, Writing – original draft, Visualization, Validation, Software, Methodology, Formal analysis, Data curation, Conceptualization. **Bailing Li:** Writing – original draft, Validation, Resources, Investigation. **Chenyang Yan:** Visualization, Methodology, Formal analysis, Data curation. **Cong Wu:** Writing – original draft, Investigation. **Lei He:** Methodology, Conceptualization. **Jingyi Cao:** Software, Resources. **Fanglin Lu:** Supervision, Resources. **Han Chen:** Supervision, Resources, Project administration, Funding acquisition. **Wei Li:** Supervision, Project administration, Funding acquisition,

Conceptualization.

Declaration of competing interest

The authors declare that they have no known competing financial interests or personal relationships that could have appeared to influence the work reported in this paper.

Data availability

Data will be made available on request.

Acknowledgements

This work was financially supported by the National Natural Science Foundation of China (31470964) & sponsored by Program of Shanghai Academic Research Leader (22XD1404700), National Natural Science Foundation of China (81972271), Independent Research Projects, and the other funding (No. 21QNPY056). Prof. Teruo Okano and Masamichi Nakayama should be appreciated for their guidance. We also appreciate the support provided by Shanghai Key Lab of Cell Engineering.

Appendix B. Supplementary data

Supplementary data to this article can be found online at https://doi.org/10.1016/j.mtbio.2024.101035.

References

[1] N. Pardi, M.J. Hogan, M.S. Naradikian, K. Parkhouse, D.W. Cain, L. Jones, M. A. Moody, H.P. Verkerke, A. Myles, E. Willis, C.C. Labranche, D.C. Montefiori, J. L. Lobby, K.O. Saunders, H.-X. Liao, B.T. Korber, L.L. Sutherland, R.M. Scearce, P. T. Hraber, I. Tombácz, H. Muramatsu, H. Ni, D.A. Balikov, C. Li, B.L. Mui, Y. K. Tam, F. Krammer, K. Karikó, P. Polacino, L.C. Eisenlohr, T.D. Madden, M. J. Hope, M.G. Lewis, K.K. Lee, S.-L. Hu, S.E. Hensley, M.P. Cancro, B.F. Haynes, D. Weissman, Nucleoside-modified mRNA vaccines induce potent T follicular helper and germinal center B cell responses, J. Exp. Med. 215 (2018) 1571–1588.

[2] N. Pardi, C.C. Labranche, G. Ferrari, D.W. Cain, I. Tombácz, R.J. Parks, H. Muramatsu, B.L. Mui, Y.K. Tam, K. Karikó, P. Polacino, C.J. Barbosa, T. D. Madden, M.J. Hope, B.F. Haynes, D.C. Montefiori, S.-L. Hu, D. Weissman, Characterization of HIV-1 nucleoside-modified mRNA vaccines in rabbits and rhesus macaques, Mol. Ther. Nucleic Acids 15 (2019) 36–47.

[3] U. Sahin, A. Muik, E. Derhovanessian, I. Vogler, L.M. Kranz, M. Vormehr, A. Baum, K. Pascal, J. Quandt, D. Maurus, S. Brachtendorf, V. Lörks, J. Sikorski, R. Hilker, D. Becker, A.-K. Eller, J. Grützner, C. Boesler, C. Rosenbaum, M.-C. Kühnle, U. Luxemburger, A. Kemmer-Brück, D. Langer, M. Bexon, S. Bolte, K. Karikó, T. Palanche, B. Fischer, A. Schultz, P.-Y. Shi, C. Fontes-Garfias, J.L. Perez, K. A. Swanson, J. Loschko, I.L. Scully, M. Cutler, W. Kalina, C.A. Kyratsous, D. Cooper, P.R. Dormitzer, K.U. Jansen, Ö. Türeci, COVID-19 vaccine BNT162b1 elicits human antibody and TH1 T cell responses, Nature 586 (2020) 594–599.

[4] C. Sheng, J. Zhao, Z. Di, Y. Huang, Y. Zhao, L. Li, Spatially resolved in vivo imaging of inflammation-associated mRNA via enzymatic fluorescence amplification in a molecular beacon, Nat. Biomed. Eng. 6 (2022) 1074–1084.

[5] Z. Xiang, J. Zhao, D. Yi, Z. Di, L. Li, Peptide nucleic acid (PNA)-Guided peptide engineering of an aptamer sensor for protease-triggered molecular imaging, Angew. Chem. Int. Ed. 60 (2021) 22659–22663.

[6] S. Mura, J. Nicolas, P. Couvreur, Stimuli-responsive nanocarriers for drug delivery, Nat. Mater. 12 (2013) 991–1003.

[7] S.T. Tucci, A. Kheirolomoom, E.S. Ingham, L.M. Mahakian, S.M. Tam, J. Foiret, N. E. Hubbard, A.D. Borowsky, M. Baikoghli, R.H. Cheng, K.W. Ferrara, Tumor-specific delivery of gemcitabine with activatable liposomes, J. Contr. Release 309 (2019) 277–288.

[8] K. Maruyama, Intracellular targeting delivery of liposomal drugs to solid tumors based on EPR effects, Adv. Drug Deliv. Rev. 63 (2011) 161–169.

[9] L.M. Hemmingsen, B. Giordani, A.K. Pettersen, B. Vitali, P. Basnet, N. Škalko-Basnet, Liposomes-in-chitosan hydrogel boosts potential of chlorhexidine in biofilm eradication in vitro, Carbohydrate Polym. 262 (2021) 117939.

[10] W.T. Al-Jamal, K. Kostarelos, Liposomes: from a clinically established drug delivery system to a nanoparticle platform for theranostic nanomedicine, Acc. Chem. Res. 44 (2011) 1094–1104.

[11] U. Bulbake, S. Doppalapudi, N. Kommineni, W. Khan, Liposomal formulations in clinical use: an updated review, Pharmaceutics 9 (2017) 12.

[12] X. Cao, C. Yang, X. Zhu, M. Zhao, Y. Yan, Z. Huang, J. Cai, J. Zhuang, S. Li, W. Li, B. Shen, Synergistic enhancement of chemotherapy for bladder cancer by photothermal dual-sensitive nanosystem with gold nanoparticles and PNIPAM, Chin. Chem. Lett. (2023) 109199.

[13] B.S. Pattni, V.V. Chupin, V.P. Torchilin, New developments in liposomal drug delivery, Chem. Rev. 115 (2015) 10938–10966.

[14] G.T. Noble, J.F. Stefanick, J.D. Ashley, T. Kiziltepe, B. Bilgicer, Ligand-targeted liposome design: challenges and fundamental considerations, Trends Biotechnol. 32 (2014) 32–45.

[15] X. Mao, J. Liu, Z. Gong, H. Zhang, Y. Lu, H. Zou, Y. Yu, Y. Chen, Z. Sun, W. Li, B. Li, J. Gao, Y. Zhong, iRGD-conjugated DSPE-PEG2000 nanomicelles for targeted delivery of salinomycin for treatment of both liver cancer cells and cancer stem cells, Nanomedicine 10 (2015) 2677–2695.

[16] S.A. Moosavian, A. Sahebkar, Aptamer-functionalized liposomes for targeted cancer therapy, Cancer Lett. 448 (2019) 144–154.

[17] J.J. Sonju, A. Dahal, S.S. Singh, S.D. Jois, Peptide-functionalized liposomes as therapeutic and diagnostic tools for cancer treatment, J. Contr. Release 329 (2021) 624–644.

[18] F. Martín-Saavedra, E. Ruiz-Hernández, C. Escudero-Duch, M. Prieto, M. Arruebo, N. Sadeghi, R. Deckers, G. Storm, W.E. Hennink, J. Santamaría, N. Vilaboa, Lipogels responsive to near-infrared light for the triggered release of therapeutic agents, Acta Biomater. 61 (2017) 54–65.

[19] A.G. Arranja, V. Pathak, T. Lammers, Y. Shi, Tumor-targeted nanomedicines for cancer theranostics, Pharmacol. Res. 115 (2017) 87–95.

[20] J. Grabowska, A.J. Affandi, D. van Dinther, M.K. Nijen Twilhaar, K. Olesek, L. Hoogterp, M. Ambrosini, D.A.M. Heijnen, L. Klaase, A. Hidalgo, K. Asano, P. R. Crocker, G. Storm, Y. van Kooyk, J.M.M. den Haan, Liposome induction of CD8+ T cell responses depends on CD169+ macrophages and Batf3-dependent dendritic cells and is enhanced by GM3 inclusion, J. Contr. Release 331 (2021) 309–320.

[21] J. Li, S. Zhou, J. Yu, W. Cai, Y. Yang, X. Kuang, H. Liu, Z. He, Y. Wang, Low dose shikonin and anthracyclines coloaded liposomes induce robust immunogenetic cell death for synergistic chemo-immunotherapy, J. Contr. Release 335 (2021) 306–319.

[22] A. Mizutani, A. Kikuchi, M. Yamato, H. Kanazawa, T. Okano, Preparation of thermoresponsive polymer brush surfaces and their interaction with cells, Biomaterials 29 (2008) 2073–2081.

[23] S. Mitragotri, T. Lammers, Y.H. Bae, S. Schwendeman, S. De Smedt, J.-C. Leroux, D. Peer, I.C. Kwon, H. Harashima, A. Kikuchi, Y.-K. Oh, V. Torchilin, W. Hennink, J. Hanes, K. Park, Drug delivery research for the future: expanding the Nano horizons and beyond, J. Contr. Release 246 (2017) 183–184.

[24] S. Komatsu, M. Tago, Y. Ando, T.-A. Asoh, A. Kikuchi, Facile preparation of multi-stimuli-responsive degradable hydrogels for protein loading and release, J. Contr. Release 331 (2021) 1–6.

[25] K. Nagase, S.F. Yuk, J. Kobayashi, A. Kikuchi, Y. Akiyama, H. Kanazawa, T. Okano, Thermo-responsive protein adsorbing materials for purifying pharmaceutical protein on exposed charging surface, J. Mater. Chem. 21 (2011) 2590–2593.

[26] J. Yu, X. He, Z. Wang, Y. Wang, S. Liu, X. Li, Y. Huang, Combining PD-L1 inhibitors with immunogenic cell death triggered by chemo-photothermal therapy via a thermosensitive liposome system to stimulate tumor-specific immunological response, Nanoscale 13 (2021) 12966–12978.

[27] M. Abri Aghdam, R. Bagheri, J. Mosafer, B. Baradaran, M. Hashemzaei, A. Baghbanzadeh, M. de la Guardia, A. Mokhtarzadeh, Recent advances on thermosensitive and pH-sensitive liposomes employed in controlled release, J. Contr. Release 315 (2019) 1–22.

[28] M. Regenold, J. Steigenberger, E. Siniscalchi, M. Dunne, L. Casettari, H. Heerklotz, C. Allen, Determining critical parameters that influence in vitro performance characteristics of a thermosensitive liposome formulation of vinorelbine, J. Contr. Release 328 (2020) 551–561.

[29] P. Cressey, M. Amrahli, P.-W. So, W. Gedroyc, M. Wright, M. Thanou, Image-guided thermosensitive liposomes for focused ultrasound enhanced co-delivery of carboplatin and SN-38 against triple negative breast cancer in mice, Biomaterials 271 (2021) 120758.

[30] M.A. Santos, S.-K. Wu, M. Regenold, C. Allen, D.E. Goertz, K. Hynynen, Novel fractionated ultrashort thermal exposures with MRI-guided focused ultrasound for treating tumors with thermosensitive drugs, Sci. Adv. 6 (2020) eaba5684.

[31] M. Dunne, B. Epp-Ducharme, A.M. Sofias, M. Regenold, D.N. Dubins, C. Allen, Heat-activated drug delivery increases tumor accumulation of synergistic chemotherapies, J. Contr. Release 308 (2019) 197–208.

[32] Y. Deng, J. Ling, M.-H. Li, Physical stimuli-responsive liposomes and polymersomes as drug delivery vehicles based on phase transitions in the membrane, Nanoscale 10 (2018) 6781–6800.

[33] H.-C. Tsai, H.-Y. Chou, S.-H. Chuang, J.-Y. Lai, Y.-S. Chen, Y.-H. Wen, L.-Y. Yu, C.-L. Lo, Preparation of immunotherapy liposomal-loaded thermal-responsive hydrogel carrier in the local treatment of breast cancer, Polymers 11 (2019) 1592.

[34] H. Bi, J. Xue, H. Jiang, S. Gao, D. Yang, Y. Fang, K. Shi, Current developments in drug delivery with thermosensitive liposomes, Asian J. Pharm. Sci. 14 (2019) 365–379.

[35] W. Li, M. Nakayama, J. Akimoto, T. Okano, Effect of block compositions of amphiphilic block copolymers on the physicochemical properties of polymeric micelles, Polymer 52 (2011) 3783–3790.

[36] X. Zhu, Y. Sun, D. Chen, J. Li, X. Dong, J. Wang, H. Chen, Y. Wang, F. Zhang, J. Dai, R.P. Pirraco, S. Guo, A.P. Marques, R.L. Reis, W. Li, Mastocarcinoma therapy synergistically promoted by lysosome dependent apoptosis specifically evoked by 5-Fu@nanogel system with passive targeting and pH activatable dual function, J. Contr. Release 254 (2017) 107–118.

[37] P. Cao, X. Sun, Y. Liang, X. Gao, X. Li, W. Li, Z. Song, W. Li, G. Liang, Gene delivery by a cationic and thermosensitive nanogel promoted established tumor growth inhibition, Nanomedicine 10 (2015) 1585–1597.

[38] W. Li, S. Feng, Y. Guo, Tailoring polymeric micelles to optimize delivery to solid tumors, Nanomedicine 7 (2012) 1235–1252.

[39] W. Li, S.-S. Feng, Y. Guo, Block copolymer micelles for nanomedicine, Nanomedicine 7 (2012) 169–172.
[40] J. Gao, Y. Yu, Y. Zhang, J. Song, H. Chen, W. Li, W. Qian, L. Deng, G. Kou, J. Chen, Y. Guo, EGFR-specific PEGylated immunoliposomes for active siRNA delivery in hepatocellular carcinoma, Biomaterials 33 (2012) 270–282.
[41] W. Li, J. Li, J. Gao, B. Li, Y. Xia, Y. Meng, Y. Yu, H. Chen, J. Dai, H. Wang, Y. Guo, The fine-tuning of thermosensitive and degradable polymer micelles for enhancing intracellular uptake and drug release in tumors, Biomaterials 32 (2011) 3832–3844.
[42] H.-F. Chow, C.-F. Leung, W. Li, K.-W. Wong, L. Xi, Synthesis and characterization of dendritic necklaces: a class of outer-sphere–outer-sphere connected dendronized organoplatinum polymers, Angew. Chem. 115 (2003) 5069–5073.
[43] W. Li, H. Zhao, W. Qian, H. Li, L. Zhang, Z. Ye, G. Zhang, M. Xia, J. Li, J. Gao, B. Li, G. Kou, J. Dai, H. Wang, Y. Guo, Chemotherapy for gastric cancer by finely tailoring anti-Her2 anchored dual targeting immunomicelles, Biomaterials 33 (2012) 5349–5362.